Divergence in a stress-associated gene regulatory network underlies differential growth control in the Brassicaceae family

Authors: Ying Sun[1*], Dong-Ha Oh[2*], Lina Duan[1], Prashanth Ramachandran[1], Andrea Ramirez[1], Anna Bartlett[3], Maheshi Dassanayake[2], José R Dinneny[1#]

Affiliations

1 Department of Biology, Stanford University, 371 Jane Stanford Way, Stanford, CA 94305, USA
2 Department of Biological Sciences, Louisiana State University, Baton Rouge, LA, 70803, USA
3 Genomic Analysis Laboratory, Salk Institute for Biological Studies, La Jolla, CA, USA
* These authors contributed equally to this work.
Correspondence should be addressed to dinneny@stanford.edu.

Abstract

The use of marginal lands in agriculture is increasingly necessary to support the global human population. Elevated salinity frequently occurs in degraded soils and hinders their use due to the negative impact salt stress has on plant growth. While the hormonal networks controlling growth have been extensively characterized in stress-sensitive plants, it is unclear how these pathways are rewired in plants that maintain growth in extreme environments. We have compared the physiological and molecular responses of four closely related members of the Brassicaceae family including two salt-tolerant species (*Shrenkiella parvula* and *Eutrema salsugineum*) and two salt-sensitive species (*Sisymbrium irio* and *Arabidopsis thaliana*) to the salt stress-induced hormone, abscisic acid (ABA). While ABA inhibits root growth in most species, we uncovered substantial growth-promoting effects in *Shrenkiella parvula*, due to an enhancement in cell elongation. Comparative transcriptomics informed by phylogenetic relationships uncovered lineage and extremophile-specific differences in ABA response. DNA Affinity Purification followed by sequencing (DAP-Seq) was utilized to establish gene regulatory networks (GRNs) in each species for the entire ABA-RESPONSIVE ELEMENT BINDING FACTORS (AREB/ABF) clade. Comparative GRN analysis identified relative conservation in the core ABA signaling GRN, while the auxin growth-hormone GRN was highly divergent, revealing how patterns of gain and loss of cis-regulatory elements mediate novel physiological outcomes. Our findings demonstrate that the targets of hormone signaling pathways are highly divergent between species and that diametric inversion of growth regulation is possible, even between closely related species of the same plant family.

Keywords: abscisic acid, extremophile, AREB/ABF, DAP-Seq, halophyte, Brassicaceae

Introduction

The survival of all organisms depends on their ability to appropriately respond to environmental signals, which is superbly exemplified by plants, whose physiology and growth is constantly tuned to suit the context [1]. During periods of environmental stress, some plants are better able to cope than others [2]. The most widely characterized plants are typically stress-sensitive, such as the molecular-genetic model *Arabidopsis thaliana* (At) and domesticated crops. Our limited knowledge of the most effective response strategies to stress currently limits our ability to maintain agricultural yields in the face of global climate change [3].

Extremophytes (stress-tolerant plants) are plant species that have evolved mechanisms to cope with various abiotic stresses such as cold, drought, and hypersaline conditions [4 5]. Recently, the reduced cost of sequencing has provided new opportunities to study the genes that underlie these physiological adaptations to extreme environments (**Fig. 1b**) [6 7]. Within the Brassicaceae, two halophyte plant species exhibit greater tolerance to soil salinity than the model plant At. *Eutrema salsugineum* (Es) is tolerant to the effects of salt and grows along the ocean shorelines of Shandong province in China, while *Schreinkiella parvula* (Sp) grows near Lake Tuz in Turkey, and is tolerant to high levels of Na^+, Li^+, Mg^{2+}, and Boron [8 9]. While At belongs to Lineage I of the Brassicaceae family, both extremophytes belong to lineage II, which also contains the stress-sensitive species *Sisymbrium irio* (Si)[10]. These species, being diploid, with small genomes, and similar numbers of genes, present new opportunities to understand how stress-mediated gene networks in extremophytes differ from stress-sensitive plants [11 12].

While salt tolerance in Es has been previously associated with strategies that maintain growth including effective energy use, regulation of excess electron flow, protective barriers in the root, and chloroplast protection, salt tolerance in Sp is less well understood [13 14]. Many environmental stressors lead to the synthesis and activation of the abscisic acid (ABA) plant hormone signaling pathway. In At, ABA inhibits germination, root growth, and gas exchange as a means of limiting growth under abiotic stress and preserving resources [15 16 17].

ABA perception triggers a signaling cascade that leads to the phosphorylation of bZIP transcription factors (TFs) known as ABA-RESPONSIVE ELEMENT BINDING FACTORS (AREB/ABFs) [18 19]. ABFs relocalize to the nucleus and activate gene expression by binding to cis-regulatory elements (CREs) known as *ABA-RESPONSIVE ELEMENT*s (*ABRE*) (**Fig. 1a**). Thousands of genes, in various tissues, are activated upon ABA treatment to confer its physiological effects in At. We hypothesized that

77 defining how the architecture of the ABA-mediated gene network varies across species
78 will elucidate whether environmental-response programs become tuned to extreme
79 environments over evolutionary timescales [20].
80
81 In this study, we examined the sensitivities of the extremophytes to exogenous ABA
82 treatment and uncovered substantial differences, most notably in Sp. We conducted
83 RNA-Seq to capture the transcriptional profile of both root and shoot tissue at short and
84 long time points to identify genes and pathways that support plant growth during stress
85 conditions. We also performed DAP-Seq to characterize the transcription factor binding
86 landscape that mediates the physiological effects of ABA signaling. We applied a
87 method we termed, swap-DAP to determine the contribution of cis- and trans-regulation
88 on the transcription factor binding landscape defined by DAP-Seq. Finally, we combined
89 these data into gene networks to define conserved and species-specific components of
90 the ABRE/ABF-mediated gene regulatory network and identify genes and subnetworks
91 that may be important for stress tolerance in extremophytes. Together, this work has
92 revealed the patterns of variation that differentiate stress tolerant and sensitive species
93 and identify specific rewiring events that allow Sp to maintain growth despite a stressful
94 environment.

95 **Results**

96 *A comparison of the growth response to ABA treatment reveals a diametric switch in the*
97 *behavior of Sp roots.*

98 ABA mediates the regulation of root growth under salinity and drought. We
99 hypothesized that studying the effects of ABA on root growth would therefore be a
100 useful approach for interrogating variation in stress response pathways and would avoid
101 the challenge of comparing transcriptional programs between species using different
102 stress treatment regimes. As was previously described, we found that At and Si root
103 growth is dramatically inhibited under elevated concentrations of NaCl, while Sp and Es
104 exhibit substantial tolerance to these effects (**Fig. 1c**). In contrast, the application of
105 exogenous ABA revealed that these treatments had inhibitory effects on primary root
106 growth in all species except Sp, which exhibited a striking promotion of growth at all
107 concentrations tested (**Fig. 1d**). We characterized the developmental basis for the
108 observed growth enhancement (**Fig. 1e**) and found that while the meristem size for At
109 and Sp is reduced upon ABA treatment (**Fig. 1f**), final cell length for Sp increased by
110 50% (from ~100 μm to ~200 μm) after treatment while no changes occurred in At (**Fig.**
111 **1g-h**). These data show that all species tested respond to ABA by differential growth,
112 but that the direction of this effect can vary dramatically depending on the species and
113 developmental context.

114 *Comparative transcriptomics informed by phylogenetic relationships uncovered lineage*
115 *and extremophyte-specific differences in ABA response*

116 To more broadly establish how responses to ABA might vary, we performed RNA-Seq
117 on the roots and shoots of all 4 species, either treated with mock or 10 μM ABA, and
118 harvested tissues at 3 hours and 24 hours post-treatment. While we captured known
119 ABA response genes in At and observed the greatest number of genes differentially
120 expressed (DE) at 3 hours in the root for At, Si, and Es, Sp again stood out with an
121 almost equal number of DE genes in both 3 hours and 24 hours root samples, while the
122 greatest number of genes in Sp appear in the shoot at 24 hours (**Fig. 2a**). Upon
123 clustering DE genes in each species and ranking the clusters from greatest to the
124 fewest number of genes within each cluster, Sp again appears to exhibit striking
125 differences in cluster patterns (**Fig. 2b**). While we identified a subset of species-specific
126 genes, the greater proportion of genes have *Arabidopsis* orthologs which facilitates a
127 cross-species comparison of gene regulation (**Fig. 2c, Supplementary Dataset 1**).
128 Using CLfinder, we defined 15,198 unambiguously 1-to-1 orthologous gene groups
129 across our four species (**Supplementary Fig. 1, Supplementary Dataset 1,2**). We
130 categorized ABA-responsive genes based on whether they showed broad conservation
131 or were regulated in a lineage, species, or extremophile-specific manner. In ranking
132 these categories, we found that conserved responses were the least prevalent while
133 stress-sensitive or extremophyte associated responses were the most prevalent (**Fig.
134 2d**). We identified patterns of GO category enrichment for DE genes (DEGs) on a per-
135 species basis, contrasting ABA-induced and repressed DEGs. Among ABA-induced
136 DEGs, we found an extensive overrepresentation of “response to abiotic stimulus” and
137 10 related non-redundant GO terms in all samples and species (**Supplementary Fig. 2,
138 Supplementary Dataset 3**). These GO terms cumulatively accounted for 20 to 25% of
139 ABA-induced DEGs in all samples and were not detected among ABA-repressed DEGs.
140

141 The phylogenetic relationship of species studied here provides an opportunity to
142 systematically detect lineage-specific modifications in pathway regulation. To identify
143 such patterns, we developed a phylogenetically informed profiling (PiP) approach that
144 utilizes a correlation metric to establish whether pairs of species exhibit a similar
145 regulatory program for genes associated with a particular Gene Ontology (GO) category
146 (**Supplementary Fig. 3a, Supplementary Dataset 4**). The GO term “response to
147 abscisic acid” showed significant correlations in all species pairs indicating broad
148 conservation in the valence of gene regulation, likely inherited from the last common
149 ancestor (**Fig. 2e**)**.** In contrast, orthologous gene pairs associated with protein
150 translation (“peptide biosynthetic process”) exhibited no correlation, or showed
151 anticorrelation, between Sp and other species in root tissues 3 hours post ABA
152 treatment. This pattern suggests an Sp-specific change in regulation (**Fig. 2f**). Several
153 GO terms related to ribosomal function and translation showed the largest variances of

154 Spearman correlation coefficient (ρ) among species pairs, especially in root samples,
155 suggesting divergence in the responses of Sp orthologs to ABA (**Supplementary Fig.**
156 **3b**). Protein translation is finely orchestrated with the metabolic activity in cells and
157 corresponds to the growth cellular state [21]. Our data suggest that Sp interprets ABA
158 signaling as a proxy for environmental stimuli where growth is enhanced, rather than
159 suppressed as it is in all other species examined here.
160
161 To profile the factors that drive differential gene expression across species, we
162 analyzed the promoters of highly ABA-responsive DEGs (fold-change ≥ 2) using
163 Analysis of Motif Enrichment (AME) (McLeay and Bailey 2010). In looking for over-
164 represented TF binding motifs within 1 Kb of upstream DNA sequence of the promoter
165 region, we found motifs for ABF1/2/3/4 and an additional 32 TFs, all of which included a
166 G-box like motif similar to the previously defined ABRE motif 22 (Supplementary Fig. 4,
167 Supplementary Dataset 5). Interestingly, none of these motifs were found enriched in
168 the promoters of ABA-repressed DEGs suggesting these motifs are associated with
169 transcriptional activators. Considering patterns of enrichment in gene functions and
170 known regulatory motifs, we hypothesized that ABA primarily acts first on the up-
171 regulation of gene expression through binding of ABFs, while the signal diversifies
172 through ABF GRNs to create more intricate responses depending on the tissue and
173 temporal contexts.

174 *The gain and loss of ABREs at the nucleotide level led to differences in the binding*
175 *landscape of ABFs*

176 To understand the molecular mechanism underlying the divergence in ABA-induced
177 transcriptional changes across species, we sought to establish global maps of ABF
178 binding in Sp, Si, Es, and At. The recent development of DNA affinity purification (DAP-
179 Seq) provided a method amendable for the study of non-model organisms. In contrast
180 with ChIP-Seq, DAP-Seq facilitates the direct measurement of TF to genomic DNA
181 (gDNA) binding without the need to develop TF-specific antibodies or generate
182 transgenic lines with epitope-tagged TFs [23]. Fortuitously, ABFs have 4 homologs within
183 each of our model species and 4 paralogs across each species (**Supplementary Fig.**
184 **5**). Therefore 16 ABFs were characterized for their ability to bind to the At genome as
185 well as the genomes of Es, Si, and Sp. A minimum of 2 biological replicates were used
186 for each pull-down and purified genomic DNA from shoot tissue was used in all cases
187 due to the low-quality of data obtained using root-derived gDNA. Stringent criteria were
188 established to ensure a high level of quality amongst the processed samples.
189 (**Supplementary Fig. 6**).
190
191 To determine if the DNA-binding affinity of ABFs varies across isoforms, we performed
192 motif analysis on the genomic regions bound by ABF using GEM [24]. Highly similar

ABRE-like motifs were identified as the most predominant binding site indicating that DAP-Seq is able to uncover the genome-wide binding landscape of ABFs across related Brassicaceae species (**Fig. 3a**). To determine the specificity of the DAP-Seq assay, we compared the proportion of ABREs occupied by DAP-Seq peaks to the distribution of the core sequence (ACGT) that centers the ABRE motif across the genome and found that ABREs as well as ABF binding occurs in higher proportion in the 5' promoter region upstream of genes compared to the ACGT sequence, which does not have a feature preference (**Supplementary Fig. 7, Supplementary Dataset 6**).

To further profile differences and similarities in the binding landscape, we compared the binding positions of the top 3000 ABF binding sites. We found significant overlap for ABFs within each species, indicating that the ABFs function redundantly to regulate downstream gene expression. To investigate the role of cis or trans effects, we swapped the cognate genome for a noncognat genome (*Arabidopsis*) during the pull-down which we termed swap-DAP. The large overlap of binding positions across species suggest that the cis-effect from the genome, instead of the TF isoform used, contributes the greatest difference in ABF binding landscape (**Fig. 3b, Supplementary Fig. 8**).

We assigned significant TF-DNA associations based on the proximity of the binding site to the nearest gene. This analysis identified 14,374 ABF-target associations for At and 10,558 for Si, 10,197 for Sp, and 20,026 for Es. These data are of particular significance as no prior information on TF-DNA interactions were available for Si, Sp, and Es. While we identified large overlaps in ABF function within species, we hypothesize that differences in ABF binding across species may rewire transcriptional responses and potentially repurpose gene networks to confer different responses to ABA. Leveraging the strength of our cross-species datasets, we characterized incidences where the ABF binding profile is altered in Sp compared to other species. For example, in AT2G21510, all ABF1/2/3/4 bind to the 5' proximal region of this gene, which is annotated as a molecular chaperone important for tolerating environmental stress. This is also true for AT5G42570, which is annotated as B-cell receptor-associated 31-like protein, previously found to be associated with cold acclimation [25]. However, while At, Si, and Es show ABF binding, Sp does not. Changes in binding profile are associated with differences in gene expression, where both AT2G21510 and AT5G42570 have greater transcript abundance under 10 μM ABA treatment in most species while the Sp orthologues have greater transcript abundance under control conditions. Our swap-Dap data set suggest that these changes are due to cis-effects since Sp ABF isoforms are able to bind these promoter regions in the At genome (**Fig 3c, Supplementary Fig. 9**). Alignment of the promoter regions across species revealed that, in the two genes highlighted from our analysis, the core ABRE motif is disrupted in Sp due to a single

base pair mutation. Interestingly, the promoters of AT2G21510 and AT5G42570 have several other ABRE-like sequences that underlie the DAP-seq peak and are fully conserved in Sp (**Fig 3d, Supplementary Fig. 10**).These other ABREs may not be sufficient to recruit ABFs due to differences in flanking sequence or higher order structural features of the locus. Thus, our analysis highlights how DAP-Seq can be used to profile functional binding site motifs and identify motif-disrupting variants that alter TF binding and target gene expression.

To test more broadly how well-correlated ABF binding is to ABA-regulated gene expression, we tested whether genes including a DAP-seq peak in adjacent genomic regions were enriched among ABA-induced and repressed DEGs. Among ABA-induced DEGs, the most significant enrichment was found for the presence of a DAP-seq peak in the 5' proximal 1Kb regions, followed by 5' distal 1Kb regions, while less to no significant enrichments were observed for a DAP-seq peak in the 3' region (**Fig 3e**). This pattern was not observed among ABA-repressed DEGs (**Supplementary Table 1**). Our method highlights the strength of comparative studies in identifying genetic variants with molecular functions which could leverage TF-binding landscapes as an emerging phenotype that can be used to connect genetic variants with differences in growth strategies.

The gain and loss of ABF-binding has led to the rewiring of GRNs controlled by ABA signaling

We hypothesized that changes in the regulation of growth by ABA is modulated by changes in the architecture of the ABF gene regulatory network (GRN) between species. To test this, we explored rewiring patterns in Sp, compared to At, by first stratifying the GRN into primary and secondary modules. We used the nodes and edges of the primary ABA network defined in Song *et al.* as a scaffold to map our DAP-Seq derived ABF edges on top [26]. We found that a majority (46/53) of the initial nodes of the network were also predicted ABF targets in At. Among these 46 genes, we found only 3 that were no longer targets of ABFs in Sp (**Supplementary Fig. 11**). Supporting these observations, we found similar transcriptional responses of these genes when comparing At and Sp, suggesting deep conservation of the ABF-mediated network.

Since ABA crosstalks with other hormone pathways, we hypothesized that divergence in the ABA GRN might also occur beyond the primary network. We focused on auxin and ethylene pathways since previous literature has shown that they cross-talk with ABA in the context of growth control [27 28 29]. We curated a list of genes with roles in biosynthesis, transport, and signaling pathways for auxin (199 genes) and ethylene (72 genes) [30 31 32 33 34 35 36 37 38 39 40](**Supplementary Fig. 11, 12**). From these datasets, we found that 33 ethylene and 81 auxin-related genes were targeted by ABFs in at least

one species (At or Sp). 18 out of 33 ethylene-related genes exhibited differences in ABF binding between At and Sp, however these changes were observed in other lineage II species as well. Among the differentially wired genes we found only 2 that are rewired in an Sp-specific manner. In contrast, we observed a larger proportion of auxin-related genes (15/81) with differences in ABF binding specifically in Sp compared to At. Additionally, we found an equal number of genes that displayed differential ABF binding in Sp and one of the other lineage II species. (**Fig. 4a**). Our transcriptome dataset is aligned with these findings and suggests a repurposing of an auxin related subnetwork since we observed many Sp orthologs displaying transcriptional patterns that could be explained by differences in ABF binding (**Fig. 4b**).

Auxin inhibits root growth by suppressing the rate of cell elongation [41]. We observed that a large number of genes that encode enzymes involved in auxin biosynthesis are rewired in the Sp ABF network (**Fig. 4a**), including *TAA1* and *YUC2*, which mediate the last steps of auxin biosynthesis. While these genes are induced by ABA in At, this effect is lost in Sp (**Fig. 4b**), suggesting that the divergence in growth regulation by ABA may, in part, be mediated by differential control of *TAA1*/*YUC2*. To validate this hypothesis, we utilized a TAA1 inhibitor, L-Kyruneine [42], to inhibit auxin biosynthesis. In At, L-Kyruneine reduced the sensitivity of roots to ABA treatment, consistent with previous work demonstrating the importance of auxin in mediating the response to ABA [43]. Similarly, the TAA1 loss of function allele *wei8-1* [44] exhibited resistance to ABA treatment (**Fig. 4c**). Together, these data suggest that ABA mediated growth inhibition depends on TAA1 and auxin biosynthesis (**Fig. 4d**). We hypothesize that in Sp, this growth inhibitory arm may be strongly diminished since the regulation of TAA1/YUC2 is no longer targeted by ABFs. Thus, the ultimate physiological outcome of ABA on primary root growth depends on the degree to which auxin biosynthesis and signaling are induced by ABF binding and transcriptional regulation.

Discussion

In our study, we aimed to investigate how stress-mediated gene networks differed between extremophytes and non-extremophile species to elucidate the components by which plants have altered ancestral networks to gain beneficial traits. We selected species in the Brassicaceae to take advantage of the extensive gene annotation and knowledge associated with *Arabidopsis*. Through transcriptional profiling and a phylogenetically informed bioinformatics approach, we were able to identify networks and pathways controlling growth with lineage-specific and species-specific differences. We found that ABFs play a large role in mediating ABA signaling since over 50% of the ABF binding sites were associated with differential expression.

Our study also highlights the first analysis conducted to explore the transcription factor binding landscape in Si, Sp, and Es as well as the use of the swap-DAP assay to distinguish between cis and trans contributions to the binding landscape. These datasets present a new resource for comparative analysis across Brassicaceae species and a model for comparative functional genomics. While our study focused on comparing 1 vs. 1 orthologs across species, these datasets can also be mined to characterize species-specific genes of unknown function and the consequence of gene duplication across species.

Using these methods, we observed several incidences where the gain or loss of ABREs near ABA-responsive genes led to differences in transcript abundance for that gene across species. This correlates with our hypothesis that the gain or loss of CREs is an important mechanism used by plants to rewire ancestral GRNs during the evolution of adaptive traits. Previous work has proven the utility of manipulating the promoter sequences of plant growth regulators to generate agriculturally beneficial traits in crops [45]. The work presented here has identified genes whose promoters have likely been the target of natural selection for extreme stress tolerance and will likely fuel the further implementation of a genetic engineering strategy for crop improvement that targets gene regulatory sequence. Future work to incorporate more Brassicaceae species into our comparative framework will better elucidate the genetic variants that define the specificity of GRNs especially in cell-type specific contexts.

ACKNOWLEDGEMENTS

We would like to acknowledge Mary Galli and Muh Ching Yee for advice on experimental design, Carnegie Institution for Science, Department of Plant Biology and Garret Huntress for providing access to computing resources and data management. Chris Pires for *S. irio* seeds. Funding was provided by the US Department of Energy's Biological and Environmental Research program (Grant DE-SC0020358, to J.R.D., D.H.O and M.D), the Carnegie Institution for Science endowment (J.R.D), National Science Foundation (MCB-1616827 and NSF-IOS-EDGE-1923589) and RDA, South Korea (Next-Generation BioGreen21 program PJ01317301) to DO and MD, and a National Science Foundation Graduate Research Fellowship (Y.S.). José Dinneny is also supported in this work as an HHMI-Simons Faculty Scholar.

AUTHOR CONTRIBUTIONS

YS, DO, MD and JRD designed the research. YS and LD performed the experiments. YS, DO, PR, AR and JRD analyzed the data. YS and JRD wrote the manuscript. DO, LD, and PR contributed to the manuscript preparation.

SUPPLEMENTARY INFORMATION

List of Supplementary Text, Figures, Tables, and Datasets

Main figure 1: *S. parvula* responds differently to ABA.
Main figure 2: RNA-Seq identifies genes regulated by ABA across species.
Main figure 3: Differences in the transcriptional response are partially due to differences in the AREB/ABF binding landscape across species.
Main figure 4: Rewiring of ABF-Auxin biosynthesis regulatory network is responsible for altered growth response in *S. parvula.*
Supp. figure 1: Genome versions used in current study and detection of all 1-to-1 ortholog groups.
Supp. figure 2: Enrichment of Gene Ontology (GO) term “response to abiotic stimulus” and related GO terms among ABA-induced Differently Expressed Genes (DEGs).
Supp. figure 3: Phylogenetically informed Profiling (PiP) analysis of ABA-responses.
Supp. figure 4: Transcription factor (TF)-binding motifs enriched among ABA-induced DEGs.
Supp. figure 5: AREB/ABFs of different species cluster together based on protein sequence and have conserved DNA-binding and protein-protein interaction domains.
Supp. figure 6: Quality control checks to confirm the DAP-Seq assay works as expected.
Supp. figure 7: Distribution of ACGT and ABRE motifs and proportions occupied by a DAP-seq peak
Supp. figure 8: Ranks and overlap of DAP-seq peaks.
Supp. figure 9: ABF binding in AT5G42570 and orthologs across species is lost in *S. parvula.*
Supp. figure 10: Core ABRE is mutated in Sp ortholog of AT5G42570.
Supp. figure 11: Integration of ABF transcription factors into hormone (ABA and Ethylene) gene regulatory networks in *S. parvula.*
Supp. figure 12: Comparison between *A. thaliana* and *S. parvula* data sets reveal changes in ABF mediated Auxin gene regulatory network.
Supplementary Table 1: Dataset of ABA-responsive genes with DAP-seq peaks among up- and down-DEGs.
Supplementary Dataset 1: All 1-to-1 Orthologous group with functional genomics data from RNA-seq and DAP-seq.
Supplementary Dataset 2: An analysis with OrthNet (including duplicates) with functional genomics data from RNA-seq and DAP-seq.
Supplementary Dataset 3: GO enrichment among ABA-induced and repressed DEGs.
Supplementary Dataset 4: Results from PiP analyses.
Supplementary Dataset 5: JASPAR motifs enriched among promoters of ABA-induced and repressed DEGs.
Supplementary Dataset 6: All DAP-seq peak coordinates with annotation (ACGT/ABRE and genomic regions), and rank.

CORRESPONDENCE

Correspondence and requests for materials should be addressed to José R. Dinneny (dinneny@stanford.edu).

MATERIALS AND METHODS

395 **Plant Material and growth conditions**
396 *Arabidopsis thaliana* Col-0 ecotype was used in this study. *Sisymbrium irio* was
397 obtained from Chris Pires, University of Missouri (KM 88-34-20-14). *Eutrema*
398 *salsugineum* ecotype Shandong and *Schrenkiella parvula* ecotype Lake Tuz were from
399 *Arabidopsis* Biological Resource Center (CS22504 and CS22663, respectively).
400
401 Seeds were surface sterilized by washing in a 95% ethanol solution for 5-min in 1.5 mL
402 Eppendorf tubes followed by a 5-min wash in a 20% bleach/ 0.1% Tween-20 solution
403 with gentle rocking at each step. Seeds were then rinsed with sterile deionized water
404 four times and stored in water for 7 days at 4°C in the dark.
405
406 After stratification, sterilized seeds were grown on 10 x 10 cm petri dish plates
407 containing sterile 0.7% Gelzan media containing ¼ x MS nutrients (MSP01-50LT;
408 Caisson), 1% sucrose, and 0.05% MES was adjusted to pH 5.7 with 1M KOH (this will
409 be termed "standard media"). The media was then sterilized using a liquid cycle for 30
410 min. 60 mL of media was used per plate.
411
412 Seedlings were grown for 6 days before transfer to standard media supplemented with
413 NaCl (Sigma-Aldrich) or ABA (Sigma- Aldrich). Methanol was used to dissolve and
414 dilute ABA to a stock solution of 100 mM and added to standard media before pouring
415 into plates. Growth of seedlings was performed in a Percival CU41L4 incubator at
416 constant temperature 24'C with light conditions 14 h light and 10 h dark at 130 µmol m^{-2}
417 s^{-1} light intensity. Plates were partially sealed with parafilm (Alcan Packaging) on three
418 sides, while the top of the plate was sealed with micropore tape (3M) to allow for gas
419 exchange. Plates were placed vertically in the chamber, so roots grow vertically along
420 the surface of the media.
421
422 For root growth assays, 20-25 seeds were placed in a row across the plate with a 1000
423 mL pipette tip. After 6 days of growth under standard media conditions, the seedlings
424 were transferred either to standard media plates again or to plates with supplements.
425 The position of the root tip was marked at the time of transfer of the root to distinguish
426 the development of the root before transfer and after transfer.
427 For tissues collected for NGS, sterilized mesh (about 10 x 10 cm squares) were first laid
428 on the media plates. 3 rows of seeds (~100 seeds) were then plated using a 1000 mL
429 pipette tip. The entire mesh would then be transferred with forceps to the plate after 6
430 days and the tissues were then separated at the root/shoot junction by a razor blade.
431
432 **Phenotypic analysis of primary root growth**
433 After seedlings are transferred to media containing various supplements, images of
434 seedlings were captured using a CanonScan 9000F flatbed scanner (Canon). Images

435 were quantified using Fiji [46]. Scale was set as 237 pixels/cm and the image was
436 measured using the segmented line tool. Two-way ANOVA and data visualization were
437 done using R.
438
439 **RNA-Seq library preparation and high-throughput sequencing**
440 Total RNA was extracted from the root and shoot tissue using RNeasy plant mini kit
441 (Qiagen 74904) according to the manufacturer's instructions for three biological
442 replicates sampled from experiments performed on a separate day. RNA quantity was
443 checked by Qubit (Q32852 Qubit® RNA Assay Kit). RNA quality of each sample was
444 assessed with a 2100 Bioanalyzer (Agilent) and fragment analyzer. RNA-Seq libraries
445 were made using NuGen Universal Plus mRNASeq according to the manufacturer's
446 instructions. Lo Bind plastic was used at every step. AMPure XP Beads (Beckman
447 Coulter, Cat A63987 or A63881) were used for the final purification steps. NuGen
448 barcodes (Barcode Version: L2V22DR) were used for multiplexing. Samples were
449 sequenced on Illumina NextSeq (single-read 75-bp run) with the multiplexed samples
450 described above on 3 lanes.
451
452 **DAP-Seq library preparation and high-throughput sequencing**
453 The coding sequence of the ABF orthologs were identified using reciprocal blast and
454 defined regions of synteny across species. Gateway cloning compatible primers will be
455 designed to amplify each coding sequence from cDNA and clone the coding sequence
456 into TOPO entry vectors [47]. Four nucleotides were added to the forward strand of the
457 primer to facilitate directional cloning. After the reaction, the plasmids were transformed
458 into chemically competent cells then grown overnight at 37ºC. Colony PCR and
459 sequencing were done to validate the cloned sequence. The confirmed entry clones
460 were then recombined into a destination vector with LR clonase to generate a vector
461 with an N-terminal HaloTag that is translationally fused to ABF. The HaloTag is a
462 mutated hydrolase that covalently binds to Halolink resin which allows for stringent
463 washing and the generation of an affinity matrix with the transcription factor [48]. We
464 found that using rabbit reticulocyte (TnT® T7 Coupled Reticulocyte Lysate System,
465 Recombinant RNasin® Ribonuclease Inhibitor- Promega) instead of wheat germ extract
466 for in vitro transcription and translation of the ABFs significantly reduces the background
467 noise and increased the quality of peaks that are able to be pulled down from DAP-
468 Seq.To confirm the successful expression and synthesis of each ABF, an immunoblot
469 with anti-halo antibody (Anti-HaloTag® Monoclonal Antibody-Promega) was performed
470 to confirm protein expression and binding efficiency for each TF. This ensures at least
471 50 ng of protein was used for each DAP-Seq pull down.
472
473 The quality of the TF- affinity matrix was assayed by using western blots to quantify the
474 abundance of the TF before and after binding to the affinity matrix. GST-Halo was used

475 as a protein standard (Promega). Incubate 1 µL of reticulocyte extract before binding
476 with beads and 2 µL of extract after the binding was used for each western on a precast
477 gel (4–20% Criterion™ TGX™ Precast Midi Protein Gel, 12+2 well, 45 µl, BioRad).
478 Before loading, Samples were mixed with Lamneii buffer and heated for 5 min at 95'C.
479 Samples were run at 20 mA for 30 min then at 100 V until the bottom was reached. 5x
480 Running buffer is made using Tris 15.1 g, Glycine 94 g, 50 mL 10% SDS. After running,
481 proteins were transferred onto the nitrocellulose membrane using a midrange, semi-dry
482 system (invitrogen). 10X TBS- 1L (80 g NaCl, 2 g KCL, 30 g Tris base, pH 8 with HCL
483 autoclave for 30 min was diluted to 1X TBST with 0.05% Tween-20 and sodium azide.
484 This was mixed with milk powder to make a 5% blocking buffer. The membrane was
485 blocked for at least 1 hour at room temperature or overnight at 4'C. After 152 blocking,
486 10 µL of anti-halo was added to 15mL blocking buffer (10 µg) for primary antibody
487 incubation. After incubation, the membrane was washed 5x for 5 min each in 1x TBST.
488 The membrane was then incubated for 1 hour with secondary anti-mouse- HRP
489 1:10,000 in 5% milk-TBST (2 µL in 20 mL blocking buffer). The membrane was washed
490 again 5x for 5 min each in 1x TBST. Chemiluminescent reagent in 1:1 ratio was added
491 to the membrane afterward and Chemi (ECL) signal was detected using Sapphire
492 biomolecular imager. Image processing and labeling was done in Fiji.
493
494 Shoot tissues from 6-day old seedlings were used to generate the genomic DNA library.
495 gDNA was extracted from root and shoot tissue by grinding tissues with cold mortar and
496 pestle then using DNeasy Plant Maxi Kit (Qiagen). gDNA was then concentrated using
497 ethanol precipitation. gDNA was incubated for 10-15 min with 10% NaOAC, 200% cold
498 100% ethanol. After precipitation, the sample was washed with 80% ethanol then dried
499 into a pellet then redissolved. gDNA was fractionated using the COVARIS system under
500 the settings (mode: Frequency sweeping, Duty cycle: 10%, intensity: 5, Cycles burst:
501 200, Time: 60 seconds, and number of cycles: 3). Another round of ethanol precipitation
502 is done in the same manner as above. End repair (End-it kit; epicentre cat # ER0720 or
503 ER81050- we used this one) and A-tailing (100mM dATP; bioPioneer inc, Klenow; (3'- 5'
504 exo- NEB) # M0212L (1,000 units) (5,000 U/mL) was done prior to ligating fractionated
505 gDNA with partial next-generation sequencing adaptors using Y adaptors. Y adaptors
506 were made by combining Adapter A with Adapter B then incubating the oligo mixture to
507 86'C for 2 minutes before allowing the reaction to return to room temperature.
508
509 Quality of DAP library was assayed using qPCR. 2 µL of (5 ng/µL) DNA template was
510 added to 18 µL master mix made with 4µL Phusion high Fidelity DNA polymerase
511 (M0530S, ThermoFisher), 1 µL of 10 mM dNTP, 0.4 µL of 10mM Illumina TruSeq
512 Universal primer and TruSeq Index primer, Phusion enzyme, 10x SYBR Green I (diluted
513 in DMSO), and H2O. DNA without adaptor ligation and water is used as a negative
514 control. Each sample was repeated 3x and on 384 qPCR plates. Thermocycling settings

were 2 min at 95'C, 30s at 98'C, 30 cycles of (15s at 98'C, 30 s at 60'C, 1 min at 72'C), followed by hold at 4'C. Quality of the library was assessed by looking at the amplification curve by plotting the curves in excel as CT vs relative fluorescence unit (RFU). If the curve plateaus within 10 cycles, then the library is good. However, if the curve plateaus after 20 cycles, then the library will not work in the final sequencing.

Final DNA is quantified using Qubit (broad range) and incubated with the ABF affinity matrix (Magne HaloTag beads, 20% slurry, promega, G7281 Lot 000243828, PBS, Ph 7.4 (homemade): Dissolve 8 g NaCl, 0.2 g KCL, 1.44g Na2HPO4 and 0.24 g KH2PO4 in 800 mL sterile water. Adjust pH to 7.4 with HCL. Add water to 1 liter and sterilize by autoclaving. Add 200 µL of 25 % NP40 and mix well., Magnetic rack, DYNAL magnetic bead separations, Invitrogen) to pull down genomic DNA that bind to each ABF.

Full adaptors containing unique 6 bp barcodes was ligated to each eluted fraction of gDNA and multiplexed for high-throughput Next-generation sequencing. These were originally designed by Muching Yee. Samples were sequenced on Illumina Hi-Seq (paired-read 150-bp run) with the multiplexed samples.

Genomes and the use of genomes for bioinformatic analysis

The genomes and gene models for *A. thaliana* was obtained from TAIR (Araport11), while genomes and gene models for *S. parvula* (version 2.2) and *E. salsugineum* (version 1.0) were from Phytozome (Phytozome ID 574 and 173, respectively). For *S. irio*, we updated the previously published gene models [10] with an updated version using evidence-assisted *ab initio* gene model prediction by the MAKER v. 2.31.10 (https://www.yandell-lab.org/software/maker.html) based on *S. irio* BUSCO-trained parameters [49] and RNA-seq data from the current study.

RNA-Seq data analysis

Raw reads were filtered and trimmed using TRIMGALORE which also generated FASTQ files for each of the libraries. Filtered reads were aligned to the reference genome using HISAT2 v. 2.2 and the expression of each primary gene model was estimated with StringTie v. 2.0.1 with default parameters[50]. Differentially expressed genes were estimated using DESeq2[51]. For comparative analyses, primary protein-coding gene models from the four species were compared using CLfinder pipeline[52] with MMSeqs2[53] as the aligner, to identify ortholog pairs and groups between pairs of species as well as for all four species. Gene Ontology (GO) annotation for *A. thaliana* was obtained on July 1st, 2020, from the GO consortium (http://geneontology.org/). For non-*Arabidopsis* species, protein-coding gene models that cover more than 70% of an *Arabidopsis* protein with alignment identified by MMSeqs2 with maximum sensitivity ('mmseqs -S 7.5' and e-value <0.001) were considered sharing the GO annotation with

555 the *Arabidopsis* protein. We used BiNGO[54] to identify GO terms enriched in up- and
556 down-regulated DEGs. Redundant GO terms sharing more than 80% of their members
557 were further consolidated using the GOMCL pipeline[55].
558
559 For Phylogenetically informed Profiling, we calculated Spearman's rank correlation of
560 the fold-change of ABA responses for all ortholog pairs annotated with a GO term,
561 between a pair of species. The significance of positive correlation was estimated for all
562 pairs of species, using scipy.stats.spearmanr [56] and subsequently corrected for multiple
563 testing (Bejamini-Hochberg) for all GO terms and all RNA-seq samples. Genes without
564 a DEG among their ortholog pair partners in all species, genes failed to pass the Cook's
565 distance test by DESeq2 [51], and genes showing larger than 2-fold changes with
566 adjusted *P*-value>0.05 (DESeq2), were excluded from the analysis. The matrix of
567 presence or absence of positive correlation between orthologs were superimposed to
568 the species tree, generated using the Agalma pipeline [57], to identify function- and
569 lineage(s)-specific modifications in gene regulations.
570
571 **DAP-Seq data analysis**
572 At least 5 million reads per each sample were filtered to remove adaptors, low-quality
573 reads, and reads mapping to multiple locations and aligned to respective genomes
574 using Bowtie (version 2.3). GEM version 3.4 was used for peak calling after normalizing
575 libraries to both input and empty vector controls. Only peaks with q-value <0.01 was
576 used for peak annotation.
577
578 For each ABF in each species, DAP-seq peaks from different biological replicates
579 whose center positions were within three nucleotides from each other were merged with
580 'bedtools merge' (https://bedtools.readthedocs.io/). We considered merged DAP-seq
581 peaks supported by minimum two biological replicates as high-confident ABF-binding
582 sites, and counted their occurrences, as well as co-occurrence of their center positions
583 with an ACGT-core or ABRE motif, within the 1~1kb (proximal) or 1001~2Kb (distal)
584 regions of the 5' and 3' side of each primary protein-coding gene models, using a
585 custom script (https://github.com/dinnenylab/BrassicaceaeGRN). The coordinates of all
586 high-confident ABF-binding sites are available as Supplementary Dataset 6. For
587 determining co-occupancy of DAP-seq peak positions by different ABFs (e.g. in swap
588 DAP-seq experiment), we selected two to three replicates with comparable library sizes
589 and ranked all peaks based on the sum of $-\log_{10}$ (q-values) and normalized peak heights
590 estimated by GEM across all selected replicates.
591
592 **Designing primers**
593 Primers were designed to amplify the CDS from different species. TM calculator was
594 used to check that the TM is under 72'C and within 1-2'C apart from each other. CACC

595 was added to the 5' end of the forward primer to make the PCR product compatible with
596 gateway cloning. The reverse complement of the reverse primer was checked to make
597 sure it is not complementing with overhanging sequence GTGG at the 5'end. To make
598 sure that the fused product is going to be in-frame, plasmid maps were 160 generated
599 and the sequence from the ATG of the protein to VP16 was translated using Expasy
600 protein translation. Primers were ordered from IDT and diluted to 100μM with sterile
601 water prior to use.
602
603 **Gene regulatory network**
604 To construct the gene regulatory network (GRN), we first manually curated a list of
605 genes that were involved in the perception, biosynthesis and signaling of the different
606 hormones (ABA, ethylene and auxin) as well as genes that were involved in the control
607 of cell elongation and root growth by auxin and ethylene. Among these genes, only
608 those with orthologs in the four species were considered for further analysis. The GRN
609 was constructed using BioTapestry with genes that showed a significant fold change in
610 response to ABA in at least one of the four species according to Supplementary Dataset
611 S1. To construct the GRN regulatory network for *S. parvula*, we first identified genes
612 that showed high-confidence ABF-binding, as defined in Supplementary Dataset S1, in
613 either *A. thaliana* or *S. parvula* or in both. The changes in ABF binding are represented
614 based on comparison to *A. thaliana*. For example, if a locus exhibited the presence of
615 an ABF DAP-seq peak in *A. thaliana* but lacked an ABF DAP-seq peak in *S. parvula*,
616 this was considered to be a loss of ABF binding (dotted lines). On the other hand, the
617 absence of a peak in *A. thaliana* but presence in *S. parvula* at an orthologous locus was
618 considered to be a gain in ABF binding (thick lines). The changes in position or number
619 of DAP-seq peaks were not considered for this analysis. Based on these criteria, we
620 identified changes in ABF binding that were specific to *S. parvula* and those that were
621 present in other species of lineage II. The GRNs were constructed using Biotapestry.
622
623

624 References:

625 1. Macneil, L. T. & Walhout, A. J. M. Gene regulatory networks and the role of
626 robustness and stochasticity in the control of gene expression. *Genome Res.* **21**,
627 645–657 (2011).

628 2. Kazachkova, Y. *et al.* Halophytism: What Have We Learnt From *Arabidopsis*
629 *thaliana* Relative Model Systems? *Plant Physiol.* **178**, 972–988 (2018).

630 3. Raza, A. *et al.* Impact of Climate Change on Crops Adaptation and Strategies to
631 Tackle Its Outcome: A Review. *Plants* **8**, (2019).

632 4. Shamustakimova, A. O., Leonova, T. G., Taranov, V. V., de Boer, A. H. & Babakov,

633 A. V. Cold stress increases salt tolerance of the extremophytes *Eutrema*
634 *salsugineum* (*Thellungiella salsuginea*) and Eutrema (*Thellungiella)* botschantzevii.
635 *J. Plant Physiol.* **208**, 128–138 (2017).

636 5. Mishra, A. & Tanna, B. Halophytes: Potential Resources for Salt Stress Tolerance
637 Genes and Promoters. *Front. Plant Sci.* **8**, 829 (2017).

638 6. Yang, R. *et al.* The Reference Genome of the Halophytic Plant *Eutrema*
639 *salsugineum*. *Front. Plant Sci.* **4**, 46 (2013).

640 7. Dassanayake, M. *et al.* The genome of the extremophile crucifer *Thellungiella*
641 *parvula. Nat. Genet.* **43**, 913–918 (2011).

642 8. Oh, D.-H. *et al.* Genome Structures and Transcriptomes Signify Niche Adaptation
643 for the Multiple-Ion-Tolerant Extremophyte *Schrenkiella parvula*. *Plant Physiology*
644 vol. 164 2123–2138 (2014).

645 9. MacLeod, M. J. R. *et al.* Exposure of two *Eutrema salsugineum* (*Thellungiella*
646 *salsuginea*) accessions to water deficits reveals different coping strategies in
647 response to drought. *Physiol. Plant.* **155**, 267–280 (2015).

648 10. Haudry, A. *et al.* An atlas of over 90,000 conserved noncoding sequences provides
649 insight into crucifer regulatory regions. *Nat. Genet.* **45**, 891–898 (2013).

650 11. Wang, J. *et al.* Genome-Wide Analysis of Gene Expression Provides New Insights
651 into Cold Responses in Thellungiella salsuginea. *Front. Plant Sci.* **8**, 713 (2017).

652 12. Orsini, F. *et al.* A comparative study of salt tolerance parameters in 11 wild relatives
653 of *Arabidopsis thaliana*. *J. Exp. Bot.* **61**, 3787–3798 (2010).

654 13. Xuejie, W. X. Z. P. Z. & Shoujin, Z. L. F. COMPARATIVE STUDIES ON GROWTH
655 AND PHYSIOLOGICAL REACTION OF THELLUNGIELLA SALSUGINEA UNDER
656 NaCl AND Na_2SO_4 STRESSES [J]. *Journal of Shandong Normal University*
657 *(Natural Science)* **1**, (2007).

658 14. Lee, Y. P. *et al.* Salt stress responses in a geographically diverse collection of
659 Eutrema/Thellungiella spp. accessions. *Funct. Plant Biol.* **43**, 590–606 (2016).

660 15. Cutler, S. R., Rodriguez, P. L., Finkelstein, R. R. & Abrams, S. R. Abscisic acid:
661 emergence of a core signaling network. *Annu. Rev. Plant Biol.* **61**, 651–679 (2010).

662 16. Sah, S. K., Reddy, K. R. & Li, J. Abscisic Acid and Abiotic Stress Tolerance in Crop
663 Plants. *Front. Plant Sci.* **7**, 571 (2016).

664 17. Vishwakarma, K. *et al.* Abscisic Acid Signaling and Abiotic Stress Tolerance in
665 Plants: A Review on Current Knowledge and Future Prospects. *Front. Plant Sci.* **8**,
666 161 (2017).

667 18. Yoshida, T. *et al.* Fou*rArabidopsis* AREB/ABF transcription factors function
668 predominantly in gene expression downstream of SnRK2 kinases in abscisic acid

669 signalling in response to osmotic stress. *Plant, Cell & Environment* vol. 38 35–49
670 (2015).

671 19. Yamaguchi-Shinozaki, K. & Shinozaki, K. A novel cis-acting element in an
672 *Arabidopsis* gene is involved in responsiveness to drought, low-temperature, or
673 high-salt stress. *Plant Cell* **6**, 251–264 (1994).

674 20. Sun, Y. & Dinneny, J. R. Q&A: How do gene regulatory networks control
675 environmental responses in plants? *BMC Biol.* **16**, 38 (2018).

676 21. Deprost, D. *et al.* The *Arabidopsis* TOR kinase links plant growth, yield, stress
677 resistance and mRNA translation. *EMBO Rep.* **8**, 864–870 (2007).

678 22. Fornes, O. *et al.* JASPAR 2020: update of the open-access database of
679 transcription factor binding profiles. *Nucleic Acids Research* (2019)
680 doi:10.1093/nar/gkz1001.

681 23. O'Malley, R. C. *et al.* Cistrome and Epicistrome Features Shape the Regulatory
682 DNA Landscape. *Cell* **165**, 1280–1292 (2016).

683 24. Guo, Y., Mahony, S. & Gifford, D. K. High resolution genome wide binding event
684 finding and motif discovery reveals transcription factor spatial binding constraints.
685 *PLoS Comput. Biol.* **8**, e1002638 (2012).

686 25. Vyse, K., Pagter, M., Zuther, E. & Hincha, D. K. Deacclimation after cold
687 acclimation-a crucial, but widely neglected part of plant winter survival. *J. Exp. Bot.*
688 **70**, 4595–4604 (2019).

689 26. Song, L. *et al.* A transcription factor hierarchy defines an environmental stress
690 response network. *Science* **354**, (2016).

691 27. Thole, J. M., Beisner, E. R., Liu, J., Venkova, S. V. & Strader, L. C. Abscisic acid
692 regulates root elongation through the activities of auxin and ethylene in *Arabidopsis*
693 *thaliana*. *G3* **4**, 1259–1274 (2014).

694 28. Rowe, J. H., Topping, J. F., Liu, J. & Lindsey, K. Abscisic acid regulates root growth
695 under osmotic stress conditions via an interacting hormonal network with cytokinin,
696 ethylene and auxin. *New Phytol.* **211**, 225–239 (2016).

697 29. Qin, H., He, L. & Huang, R. The Coordination of Ethylene and Other Hormones in
698 Primary Root Development. *Front. Plant Sci.* **10**, 874 (2019).

699 30. Majda, M. & Robert, S. The Role of Auxin in Cell Wall Expansion. *Int. J. Mol. Sci.*
700 **19**, (2018).

701 31. Strader, L. C., Chen, G. L. & Bartel, B. Ethylene directs auxin to control root cell
702 expansion. *Plant J.* **64**, 874–884 (2010).

703 32. Li, J., Xu, H.-H., Liu, W.-C., Zhang, X.-W. & Lu, Y.-T. Ethylene Inhibits Root
704 Elongation during Alkaline Stress through AUXIN1 and Associated Changes in

705 Auxin Accumulation. *Plant Physiol.* **168**, 1777–1791 (2015).

706 33. Takatsuka, H. & Umeda, M. Hormonal control of cell division and elongation along
707 differentiation trajectories in roots. *J. Exp. Bot.* **65**, 2633–2643 (2014).

708 34. Mao, J.-L. *et al. Arabidopsis* ERF1 Mediates Cross-Talk between Ethylene and
709 Auxin Biosynthesis during Primary Root Elongation by Regulating ASA1
710 Expression. *PLoS Genet.* **12**, e1005760 (2016).

711 35. Van den Broeck, L. *et al.* From network to phenotype: the dynamic wiring of an
712 *Arabidopsis* transcriptional network induced by osmotic stress. *Mol. Syst. Biol.* **13**,
713 961 (2017).

714 36. Yang, Z., Tian, L., Latoszek-Green, M., Brown, D. & Wu, K. *Arabidopsis* ERF4 is a
715 transcriptional repressor capable of modulating ethylene and abscisic acid
716 responses. *Plant Mol. Biol.* **58**, 585–596 (2005).

717 37. Dubois, M. *et al.* Ethylene Response Factor6 acts as a central regulator of leaf
718 growth under water-limiting conditions in *Arabidopsis*. *Plant Physiol.* **162**, 319–332
719 (2013).

720 38. Müller, M. & Munné-Bosch, S. Ethylene Response Factors: A Key Regulatory Hub
721 in Hormone and Stress Signaling. *Plant Physiol.* **169**, 32–41 (2015).

722 39. Markakis, M. N. *et al.* Identification of genes involved in the ACC-mediated control
723 of root cell elongation in *Arabidopsis thaliana*. *BMC Plant Biol.* **12**, 208 (2012).

724 40. Miao, Z.-Q. *et al.* HOMEOBOX PROTEIN52 Mediates the Crosstalk between
725 Ethylene and Auxin Signaling during Primary Root Elongation by Modulating Auxin
726 Transport-Related Gene Expression. *Plant Cell* **30**, 2761–2778 (2018).

727 41. Velasquez, S. M., Barbez, E., Kleine-Vehn, J. & Estevez, J. M. Auxin and Cellular
728 Elongation. *Plant Physiol.* **170**, 1206–1215 (2016).

729 42. Pacheco-Villalobos, D., Sankar, M., Ljung, K. & Hardtke, C. S. Disturbed local
730 auxin homeostasis enhances cellular anisotropy and reveals alternative wiring of
731 auxin-ethylene crosstalk in Brachypodium distachyon seminal roots. *PLoS Genet.*
732 **9**, e1003564 (2013).

733 43. Thole, J. M., Beisner, E. R., Liu, J., Venkova, S. V. & Strader, L. C. Abscisic acid
734 regulates root elongation through the activities of auxin and ethylene in *Arabidopsis*
735 *thaliana*. *G3: Genes, Genomes, Genetics* **4**, 1259–1274 (2014).

736 44. Stepanova, A. N. *et al.* TAA1-mediated auxin biosynthesis is essential for hormone
737 crosstalk and plant development. *Cell* **133**, 177–191 (2008).

738 45. Rodríguez-Leal, D., Lemmon, Z. H., Man, J., Bartlett, M. E. & Lippman, Z. B.
739 Engineering Quantitative Trait Variation for Crop Improvement by Genome Editing.
740 *Cell* **171**, 470–480.e8 (2017).

741 46. Schindelin, J. *et al.* Fiji: an open-source platform for biological-image analysis. *Nat.*
742 *Methods* **9**, 676–682 (2012).

743 47. Patel, B. Simple, Fast, and Efficient Cloning of PCR Products with TOPO® Cloning
744 Vectors. *BioTechniques* vol. 46 559 (2009).

745 48. England, C. G., Luo, H. & Cai, W. HaloTag technology: a versatile platform for
746 biomedical applications. *Bioconjug. Chem.* **26**, 975–986 (2015).

747 49. Waterhouse, R. M. *et al.* BUSCO Applications from Quality Assessments to Gene
748 Prediction and Phylogenomics. *Mol. Biol. Evol.* **35**, 543–548 (2018).

749 50. Pertea, M., Kim, D., Pertea, G. M., Leek, J. T. & Salzberg, S. L. Transcript-level
750 expression analysis of RNA-seq experiments with HISAT, StringTie and Ballgown.
751 *Nat. Protoc.* **11**, 1650–1667 (2016).

752 51. Love, M. I., Huber, W. & Anders, S. Moderated estimation of fold change and
753 dispersion for RNA-seq data with DESeq2. *Genome Biol.* **15**, 550 (2014).

754 52. Oh, D.-H. & Dassanayake, M. Landscape of gene transposition-duplication within
755 the Brassicaceae family. *DNA Res.* **26**, 21–36 (2019).

756 53. Steinegger, M. & Söding, J. MMseqs2 enables sensitive protein sequence
757 searching for the analysis of massive data sets. *Nat. Biotechnol.* **35**, 1026–1028
758 (2017).

759 54. Maere, S., Heymans, K. & Kuiper, M. BiNGO: a Cytoscape plugin to assess
760 overrepresentation of gene ontology categories in biological networks.
761 *Bioinformatics* **21**, 3448–3449 (2005).

762 55. Wang, G., Oh, D.-H. & Dassanayake, M. GOMCL: a toolkit to cluster, evaluate, and
763 extract non-redundant associations of Gene Ontology-based functions. *BMC*
764 *Bioinformatics* **21**, 139 (2020).

765 56. Virtanen, P. *et al.* SciPy 1.0: fundamental algorithms for scientific computing in
766 Python. *Nat. Methods* **17**, 261–272 (2020).

767 57. Dunn, C. W., Howison, M. & Zapata, F. Agalma: an automated phylogenomics
768 workflow. *BMC Bioinformatics* **14**, 330 (2013).

769

770 **Figure Legends**

771

772 **Fig.1: S. parvula responds differently to ABA. a,** ABA signaling pathway in
773 Arabidopsis. ABA functions to regulate cellular and tissue level responses to
774 environmental stress such as cold, salt, and drought. ABA signaling alters cellular
775 responses by activating the transcription of many genes. **b,** A simplified phylogenetic
776 tree representing an overview of how the diploid species from Brassicaceae relate to
777 one another and a summary of their comparative genome size, number of

778 chromosomes, and number of coding sequences. **c,d,** Quantification of primary root
779 growth of At, Si, Sp, and Es seedlings after transfer to media containing control, 100,
780 150, 200 mM NaCl (**c**), or 1, 5, 10 μM ABA (**d**) for 2 days. Asterisks mark significant
781 changes based on two-way ANOVA, $*P < 0.05$, $**P < 0.01$, $***P < 0.001$, n>6. **e,**
782 Confocal microscopy images of both At and Sp primary roots grown on standard media
783 or media containing 10 μM ABA. Blue bars label the stabilized cortex cell length. Red
784 arrows point to the end of meristem. Scale bars = 100 μm. **f,** Quantifications of root
785 meristem size, by counting the total cortex cell number within the meristem, for both At
786 and Sp under control and 1 or 10 μM ABA treatment. Significance test is based on
787 pairwise T-test, $***P < 0.001$, n = 5. **g,h,** Quantification of cortex cell length for both At
788 (**g**) and Sp (**h**) under control, 1 or 10 μM ABA treatment (n = 5). The x-axis indicates cell
789 number starting from the quiescent center (QC).
790
791 **Fig.2: RNA-Seq identifies genes regulated by ABA across species. a**, Bar chart
792 summarizing the number of differentially expressed (DE) genes across species. Log_2
793 fold change was used to quantify the total number of up and down- regulated genes for
794 each species. Only genes with a p-value <0.05 are displayed. Red indicates up-
795 regulated genes, blue indicates down-regulated genes. **b**, Heatmap of log_2 fold change
796 of differentially expressed genes. Each species was clustered separately using Ward's
797 hierarchical clustering method. Clusters are then arranged in descending order. **c**, Lists
798 of DE genes from each species are compared with DE genes from *Arabidopsis* and
799 categorized into 4 separate categories (1) Genes with ortholog in At, (2) Genes specific
800 to species, (3) Genes specific to species with phenotypes in At, (4) Genes specific to
801 species with unknown function. **d**, Cluster analysis of 1:1 Ortholog Groups (OGs) and
802 number of genes associated with each pattern. Total 15,198 1:1 OGs were defined
803 where all ortholog pairs were reciprocally best homologs among themselves
804 (**Supplementary Fig. 1**) and used to associate differential gene expression. The top 9
805 categories of gene expression are shown in descending order. Pink indicates
806 orthologous genes across species. **e,f,** Phylogenetically-informed profiling (Pip)
807 highlights the regulatory traits that show the most significant lineage(s)-specific
808 modifications. While ortholog pairs annotated with GO-term “response to abscisic acid”
809 showed significant positive Spearman correlation (ρ) of ABA-responsive expression
810 fold-changes (* adjusted $p<10^{-7}$) in all species pairs (**e**), the correlation disappeared in
811 GO term “peptide biosynthetic process” in species pairs including *S. parvula* (Sp), due
812 to a subset of Sp genes regulated in the opposite direction (yellow arrows), signifying a
813 lineage-specific modification (red arrow in the species tree) (**f**). Among all tested,
814 conserved ABA-response (**e**) was the most frequent profile (3,424 GO-sample), while
815 unique modification in Sp (**f**) was among the next most frequent (123 GO-sample)
816 (**Supplementary Fig. 3a**). The GO term “peptide biosynthetic process” in root 3hr ABA
817 treatment sample represents one of the biggest variance in ρ among larger GO terms

818 (**Supplementary Fig. 3b**) See **Supplementary Dataset 4** for Pip results for all GO
819 terms and samples.
820
821 **Fig.3: Differences in the transcriptional response are partially due to differences**
822 **in the ABF binding landscape across species. a,** Experimental set up to profile
823 differences in AREB/ABF function and target genes across species for DAP-Seq and
824 Swap-Dap. The ABRE is the enriched motif under the peaks associated with ABF
825 binding. 16 ABF orthologs are displayed based on the phylogenetic association of their
826 amino acid sequence. For each ABF, the enriched motif is represented as a position
827 weight matrix (PWM). **b**, Overlap of DAP-seq peak positions bound by ABFs. Upper
828 panel shows overlaps among top 3000 DAP-seq peak positions in each Brassicaceae
829 genome bound by ABF1/2/3/4. In the lower panel, ABFs from four Brassicaceae species
830 were applied to the *Arabidopsis thaliana* genome in swap-DAP-seq experiments. Co-
831 occupancy by ABFs from different species for top 1000 peak positions was plotted for
832 each ABF. Top DAP-seq peak positions were identified by ranking based on the
833 significance and normalized peak heights, as detailed in methods. A summary of how
834 peaks overlaps over different numbers of top peak positions is in Supplementary Fig. 6.
835 **c**, A genome browser summary to highlight an example gene where ABF binding is lost
836 in Sp but not in other species, which correlates with gene expression differences. The
837 gene IDs associated for each species are (At) AT2G21510.2, (Si) Si_s2286_00530.m,
838 (Sp) Sp4g00670.a, and (Es) Thhalv10000223m.v1.0. Y-axis on IGV coverage track is
839 adjusted for each track to show the maximum height for the depth of coverage while the
840 gene model is proportional to what is observed in a 10,000 bp window. For Sp tracks, y-
841 axis was adjusted to the lower range of 50 to confirm no peaks were present. Panels
842 show peak signal vs. empty vector and input control, differences in ABF binding across
843 species, similarities in binding sites in swap-dap data, and corresponding gene
844 expression data for transcripts. At, Si, and Es show positive $\log_2$ fold change while Sp
845 shows negative fold change upon ABA treatment. **d**, A nucleotide alignment of
846 sequences in the 5' promoter of At, Si, Sp, and Es. The reverse complement was used
847 for the alignment since the gene is in the reverse strand. Alignment was performed in
848 MUltiple Sequence Comparison by Log- Expectation (muscle). Blue boxes highlight the
849 ABRE motif. Red letter nucleotide change that leads to the mutation and loss of the core
850 ABRE motif. **e**, We tested whether genes including a DAP-seq peak in different genomic
851 regions were enriched among ABA-induced DEGs compared to genes not regulated by
852 ABA (background). Percent enrichment, compared to background, for genes
853 significantly ABA-induced in any of the four samples (up-DEG in any sample, i.e. root or
854 shoot tissues treated with ABA for 3hr or 24hr) and in all four samples (up-DEG in all
855 samples) were plotted separately. Genomic regions are divided into 5' distal (5pD), 5'
856 proximal (5pP), genomic coding sequences (gCDS), 3' proximal (3pP), and 3' distal
857 (3pD), where proximal regions are within 1Kb of the coding sequence of a gene model

858 and distal regions the next 1Kb blocks beyond the proximal regions. Significance of
859 enrichment (g-test with Benjamini-Hochberg correction) was marked for adjusted p-
860 value < 10^{-5} (*), <10^{-20} (**), and <10^{-50} (***). Significant enrichment of genes containing a
861 DAP-seq peak in most genomic regions was not observed among ABA-repressed
862 DEGs (**Supplementary Table 1**).
863
864
865 **Fig.4: Rewiring of ABF-Auxin biosynthesis regulatory network is responsible for**
866 **altered growth response in S. parvula. a**, Gene regulatory network for auxin
867 biosynthesis, transport, signaling, and cell wall are composed based on data from
868 previous published literature. A list of binding sites from ABF 1-4 were consolidated to
869 draw the gene network in Arabidopsis. Sp data was overlaid onto the Arabidopsis
870 network. Species-specific differences are highlighted as well as the presence or
871 absence of a peak based on ABF binding. **b,** Heatmap summarizing the RNA-Seq data
872 across At and Sp for species-specific and lineage-specific data highlighted in previous
873 GRN. Genes are clustered based on differences observed between At and other
874 species. **c,** Quantification of primary root growth for WT and wei8-1 mutants treated with
875 control, 1 μM ABA, as well as WT with 1μM L-Kyn, and 1 μM L-Kyn + 1 μM ABA.
876 Asterisk indicate significance by 2-way ANOVA. ∗∗∗P < 0.001, n>30. **d,** A schematic
877 mechanism we proposed for the differential regulation in primary root growth in Sp
878 compared with At.
879
880 **Supplementary Fig.1: Genome versions used in current study and detection of all**
881 **1-to-1 ortholog groups.**
882 **a,** The genome versions used as well as gene loci, percent of loci in large scaffolds, and
883 the Benchmarking Universal Single-Copy Orthologs (BUSCOs) analysis are shown
884 along with an updated gene model annotation for *Sisymbrium irio*. **b,** A schematic
885 example of OrthNet constructed for the four crucifer species. Protein-coding gene
886 models from each species were paired with their best homologs in other species. Pairs
887 of homologs were organized into OrthNet, each OrthNet representing orthologs likely
888 derived from a single ancestral locus (Oh and Dassanayake, 2019). Within each
889 OrthNet, a quartet of orthologs unambiguously find each other as reciprocal best
890 homologs is defined as "all 1-to-1 ortholog group (OG)" (red dashed box). We identified
891 15,198 all 1-to-1 OGs among the four crucifers, and used them as the framework for
892 cross-species comparisons. RNA-seq and DAP-seq results for all 1-to-1 OGs are in
893 Supplementary Dataset 1, while the same data for all genes, organized as OrthNets
894 including all duplicated paralogs, are in Supplementary Dataset 2.
895 [a] Percentage of 1,375 BUSCOs (embryophyte ortholog database version 10) detected
896 in each genome; C, Complete; S, Single-copy; D, Duplicated; F, Fragmented; M,
897 Missing BUSCOs

898 [b] Using the updated *S. irio* gene models, the number of unambiguous all-1-to-1 ortholog
899 groups in the four crucifer species increased to 15,198, compared to 14,526 when the
900 original version of *S. irio* gene models by Haudry, et al. (2013) was used.
901
902 **Supplementary Fig.2: Enrichment of Gene Ontology (GO) term "response to**
903 **abiotic stimulus" and related GO terms among ABA-induced Differentially**
904 **Expressed Genes (DEGs). a,** The GO term "response to abiotic stimulus" and ten
905 related non-redundant GO terms (presented in the heatmap in the bottom panel) were
906 the only GO terms showed significant enrichment among ABA-induced DEGs (up-
907 DEGs) in all samples, i.e. 3hr ABA treatment, root tissue (R3); 24hr, root tissue (R24);
908 3hr, shoot tissue (S3); and 24hr, shoot tissue (S24) for all species, i.e. *Arabidopsis*
909 *thaliana* (At), *Sisymbrium irio* (Si), *Schrenkiella parvula* (Sp), and *Eutrema salsugineum*
910 (Es). The top panel shows the proportion of up-DEGs that are annotated with any of the
911 "response to abiotic stimulus" and the ten related GO terms, compared to the mean
912 proportion in all genes of the four species, i.e. the background (dashed line). Bottom
913 panel shows the significance of enrichment, estimated with a hypergeometric test with
914 Benjamini-Hochberg correction as a heatmap. The entire GO terms showing enrichment
915 of any of the ABA-induced or repressed DEGs are compiled in Supplementary Dataset
916 3.
917
918
919 **Supplementary Fig. 3: Phylogenetically informed Profiling (PiP) analysis of ABA-**
920 **responses**
921 1.**a**, For all non-redundant GO terms, we determined if there is a significant positive
922 Spearman correlation (+corr) of ABA responses among ortholog pairs for all six pairs of
923 the four species, i.e. *Arabidopsis thaliana* (At), *Sisymbrium irio* (Si), *Schrenkiella parvula*
924 (Sp), and *Eutrema salsugineum* (Es). The matrix of presence (1) and absence (0) of
925 +corr was calculated for ABA-responsive fold change of gene expression in each of the
926 four samples, i.e. root and shoot tissues with 3 and 24hr ABA treatment. In panel **a**, we
927 show the number of GO-sample pairs with the indicated +corr patterns across all pairs
928 of species. The most frequent +corr pattern (3,425 GO-sample pairs) represented GO-
929 sample pairs with no modification in any lineage ("Conserved in all"). The next dominant
930 +corr pattern (123 GO-sample pairs) that matches a phylogenetic profile showed a
931 modification of ABA responses uniquely in Sp ("Unique@Sp"). Phylogenetic profiles
932 "AtEs-SiSp" mirrors the divergence of Si and Sp clades from the other two species,
933 while "AtSi-vs-SpEs" indicates potential division between glycophytes (At and Si) and
934 halophytes (Sp and Es). For all GO-sample pairs, we plotted the Variance of Spearman
935 correlation coefficients among the six species pairs against the number of ortholog pairs
936 used for PiP analyses. **b,** While in general the magnitude of variance was greater for
937 smaller GO terms, "peptide biosynthetic process" and related GO terms at root 3hr ABA

938 treatment samples were outliers with greater variances among larger GO terms (marked
939 red). Results of PiP analysis for all GO-sample pairs are in Supplementary Dataset 4.
940
941 **Supplementary Fig. 4: Transcription factor (TF)-binding motifs enriched among**
942 **ABA-induced DEGs. a,** For the 1Kb upstream regions of all ABA-induced and
943 repressed DEGs, we searched for enrichment of known TF-binding motifs (from
944 JASPAR database). The four ABFs and other G-box-binding TFs (G-box TFs) were the
945 only TFs whose known binding motifs showed significant enrichment (determined using
946 AME) in promoters of ABA-induced DEG promoters in all samples. **b,** Proportion of
947 promoters including an ABF or G-box TF-binding motif is shown in panel b, for both
948 DEGs ABA-induced (Up-DEGs) and repressed (Down-DEGs), with the mean proportion
949 among non-DEGS shown as dotted lines (G-Box TF) and dashed lines (ABFs). The
950 enrichment profiles of all JASPAR TF-binding motifs are in Supplementary Dataset 5.
951
952 **Supplementary Fig.5: AREB/ABFs of different species cluster together based on**
953 **protein sequence and have conserved DNA-binding and protein-protein**
954 **interaction domains. a,** Alignment was generated using CLUSTALW with the amino
955 acid sequences for each species. Black box highlights the conservation of the DNA
956 binding domain and the protein-protein interaction domain for ABFs across species.
957
958 **Supplementary Fig.6: Quality control checks to confirm the DAP-Seq assay works**
959 **as expected. a**, DAP-Seq peaks associated with ABI1 and RD29A, which are marker
960 genes for ABA response, are found across all species. Genome browser view shows
961 binding sites represented as “peaks”. Dotted lines connect orthologous genes across
962 species. ABREs are labeled in red and the data range for X axis was standardized to
963 10,000bp. Corresponding differential gene expression data (ABA treatment vs. control
964 from RNA-Seq for each gene ortholog across species is shown as $\log_2$ fold change. **b**,
965 Proteins synthesized by in vitro transcription/ translation (IVT) runs to expected size
966 within typical yields as described in O’Malley *et al*. anti-HALO monoclonal antisera was
967 used for detection of HALOtag used to generate the affinity matrix. GST-HALOTag
968 (Halo protein) was used as positive control.
969
970 **Supplementary Fig.7: Distribution of ACGT and ABRE motifs and proportions**
971 **occupied by a DAP-seq peak. a,** On the left panels, occurrences per kilobase (Kb) of
972 the ACGT, ACGT sequences that are not a part of an ABRE (ACGT – ABRE), and
973 ABRE motif, are plotted for different genomic regions adjacent to protein-coding gene
974 models. Genomic regions are divided into 5’ distal (5pD), 5’ proximal (5pP), genomic
975 coding sequences (gCDS), 3’ proximal (3pP), and 3’ distal (3pD), where proximal
976 regions are within 1Kb of the coding sequence of a gene model and distal regions the
977 next 1Kb blocks beyond the 1Kb regions. Intergenic regions are those not within 2Kb of

any gene model. For each motif, percent proportions occupied by an ABF-binding DAP-seq peak are shown on the right panel. Motif logos indicate the definition of ACGT and ABRE motif. Genomic coordinates of all high-confidence DAP-seq peaks, together with their coincidence with ACGT or ABRE motifs and genomic regions adjacent to protein-coding gene models, are in Supplementary Dataset 6.

Supplementary Fig. 8: Ranks and overlap of DAP-seq peaks. a, DAP-seq peaks were ranked based on significance and peak heights as detailed in Methods. We selected the top N ranked DAP-seq peaks from each experiment and compared their overlaps among ABF1/2/3/4 within each species (A) or among ABF orthologs derived from At/Si/Sp/Es for each ABF in swap DAP-seq experiment. **b,** Percentages of DAP-seq peak positions shared by all four ABFs (intersection) among all peak positions (union) were plotted over different N values.

Supplementary Fig.9: ABF binding in AT5G42570 and orthologs across species is lost in *S. parvula.*
a, genome browser view showing binding sites represented as “peaks”. Data shows loss of binding in Sp compared to binding in all other samples. The gene IDs associated for each species are (At) AT5G42570, (Si) Si_s118_00070.m, (Sp) SpUn0014_0110, and (Es) Thhalv10003268m.v1.0. Y-axis on IGV coverage track is adjusted for each track to show the maximum height for the depth of coverage while the gene model is proportional to what is observed in a 10,000 bp window. For Sp tracks, y-axis was adjusted to the lower range of 50 to confirm no peaks were present. Swap-DAP data indicates the peak loss is due to cis since SpABFs are able to bind to the 5’ promoter region in the At genome. RNA-Seq data corresponds to peak patterns where the presence of a peak suggests transcriptional activation.

Supplementary Fig.10: Core ABRE is mutated in Sp ortholog of AT5G42570
a, An alignment of sequences in the promoters of AT5G42570 and corresponding orthologs. The reverse complement for each sequence was taken since genes are in the reverse strand then aligned with MUltiple Sequence Comparison by Log-Expectation (muscle). Blue boxes indicate the ABRE motif, the red letter indicate the nucleotide sequence change in Sp at the ABRE leading to the loss of the binding site for Sp.

Supplementary Fig.11: Integration of ABF transcription factors into hormone (ABA and Ethylene) gene regulatory networks in *S. parvu*la. Gene regulatory maps were drawn using BioTapestry, with a solid arrow line indicating correlation between ABF binding (DAP-Seq) and gene expression (RNA-Seq). **a**, A Map for *Arabidopsis* ABF-mediated gene regulatory network was drawn with overlapping transcription factors

1018 and targets from ChIP-Seq (Song et al., 2016). DAP-Seq and RNA-Seq data from
1019 different species were overlaid and differences are highlighted: dotted arrow indicates
1020 loss of ABF binding, bold arrow indicates gain of ABF binding, and colors indicate
1021 differences that are lineage II specific, Sp-Si specific, Sp-Es specific, or Sp specific.
1022 Heatmap indicates differential gene expression patterns in all tissue types and time
1023 points for all nodes used to construct the GRN. **b**, An overlay of ABF-mediated GRN
1024 using ethylene regulatory network curated from previously published literature is shown.
1025 Of the 72 genes identified, 50 were responsive to ABA, and 33 had ABF DAP peaks in
1026 either At, Sp, or both which were used to construct the GRN. Among these however,
1027 only 2 were specific to Sp (ACS7 and ERF2) while the other 20 showed lineage II, Sp-
1028 Es, or Sp-Si specific differences. Heatmap indicates differential gene expression
1029 patterns in all tissue types and time points for all nodes used to construct the GRN.
1030 LFC_2 indicates log_2 fold change.
1031
1032 **Supplementary Fig.12: Comparison between *A. thaliana* and *S. parvula* data sets**
1033 **reveal changes in ABF mediated auxin gene regulatory network**. **a,** A total of 199
1034 genes were curated for the analysis. 117 of the 199 genes related to primary auxin
1035 signaling in roots were present in our RNA-Seq data. 81 of these genes had ABF DAP
1036 peaks in either At or Sp or in both suggesting ABF mediate gene regulation and shown
1037 in this GRN as nodes. The same parameters were used as in Supplementary Fig.8 to
1038 highlight lineage, Sp-Si, Sp-Es, or Sp specific differences compared to At.

Figure 1: *S. parvula* responds differently to ABA.

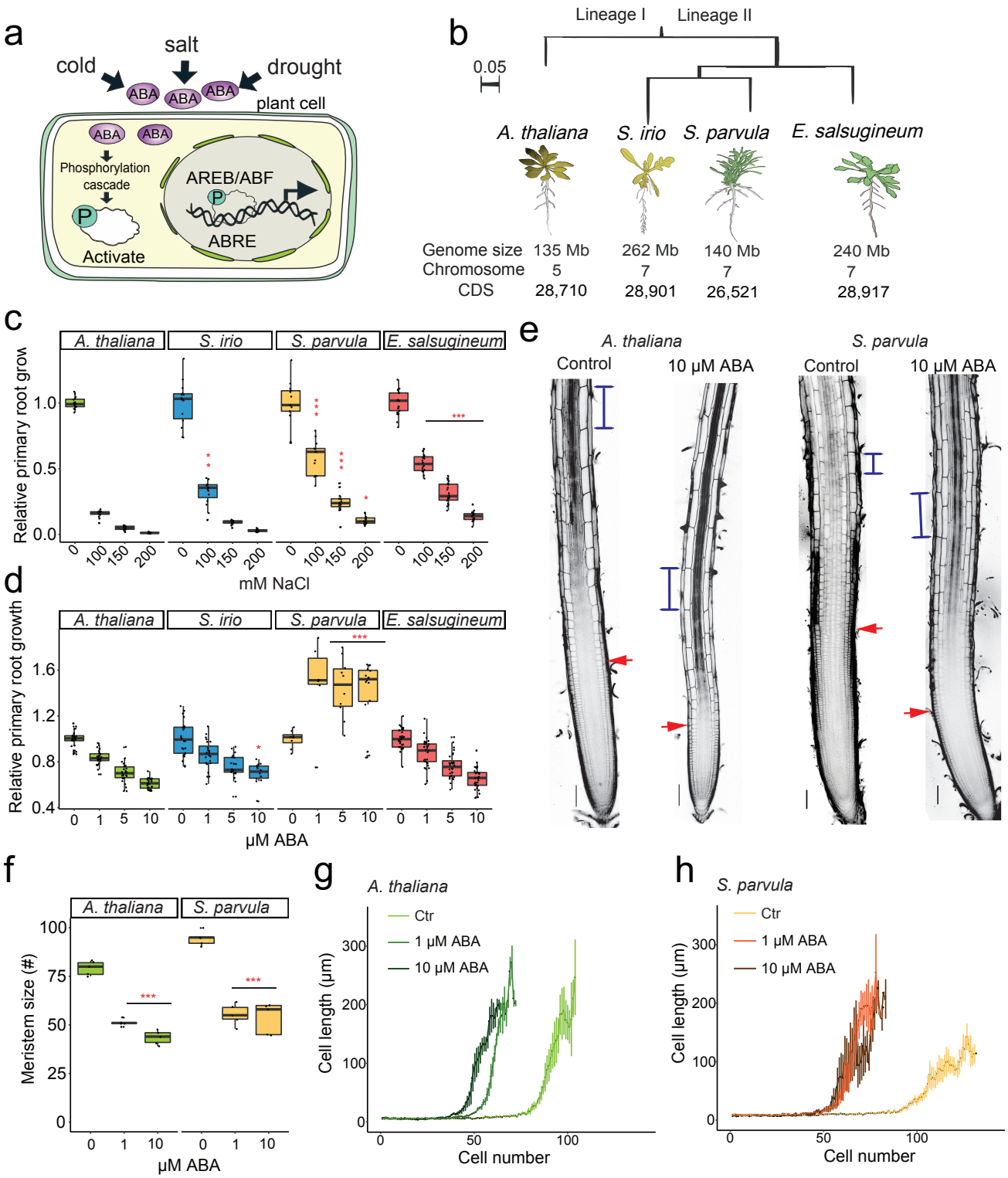

Figure 2: RNA-Seq identifies genes regulated by ABA across species.

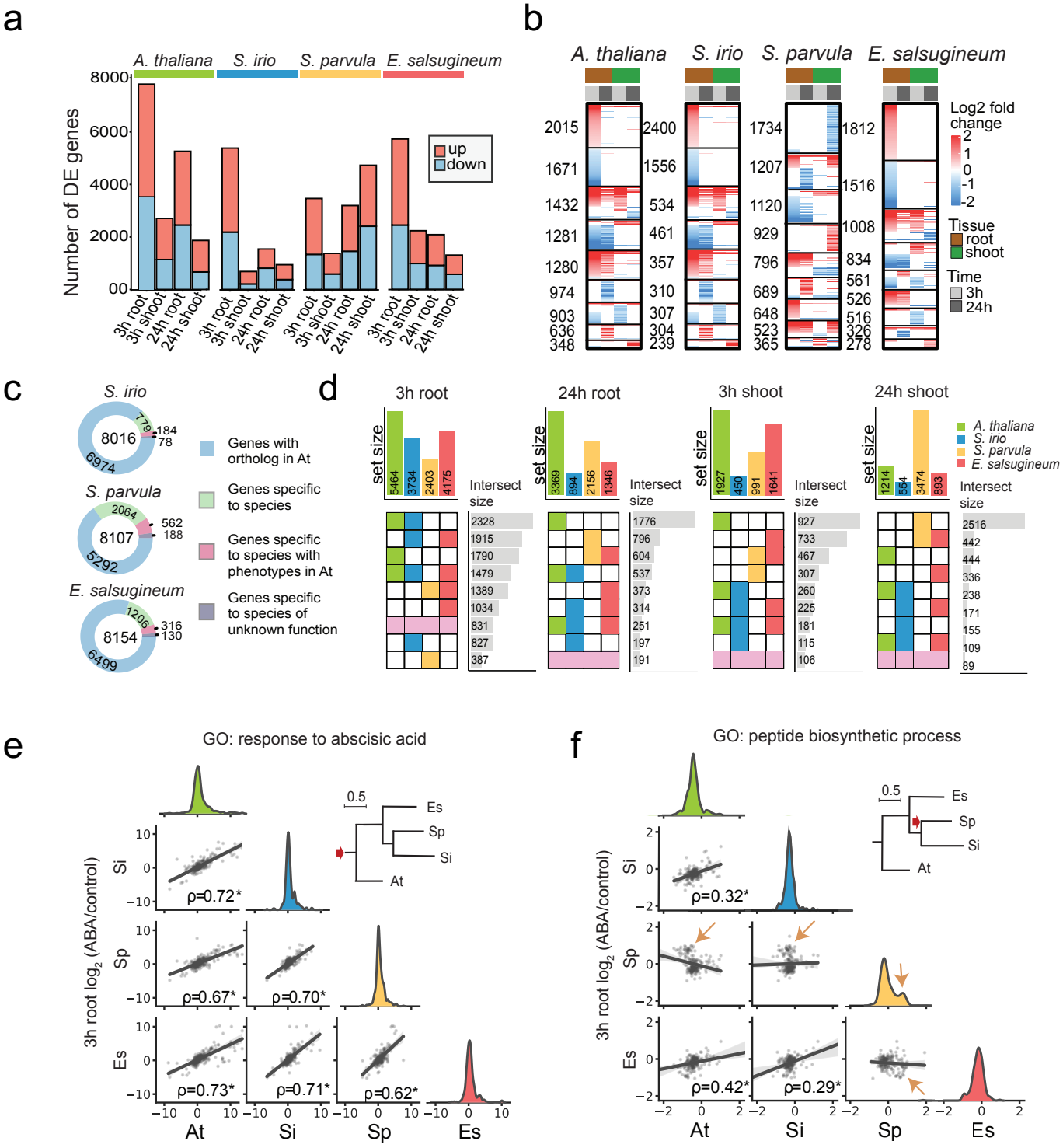

Figure 3: Differences in the transcriptional response are partially due to differences in the AREB/ABF binding landscape across species.

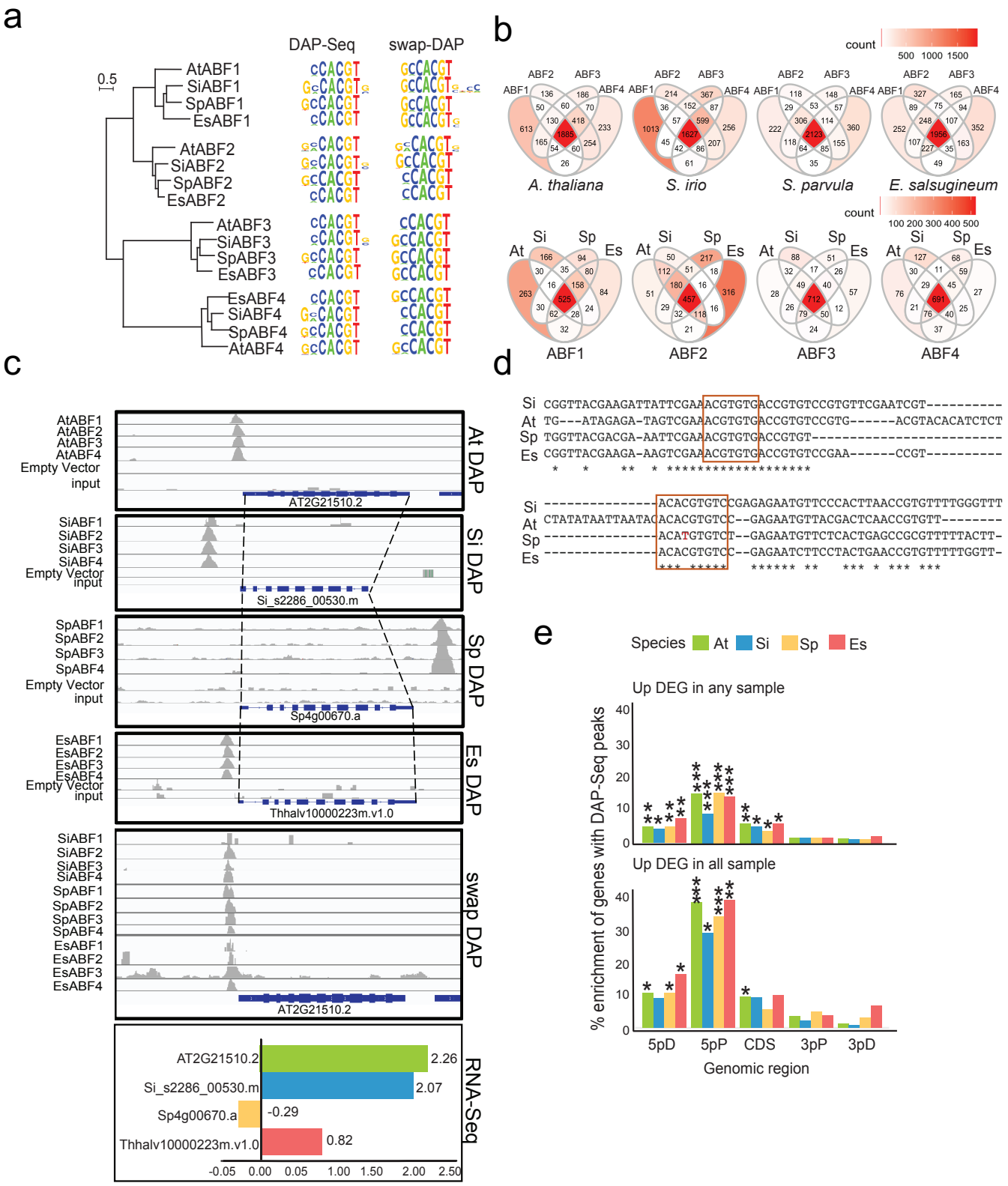
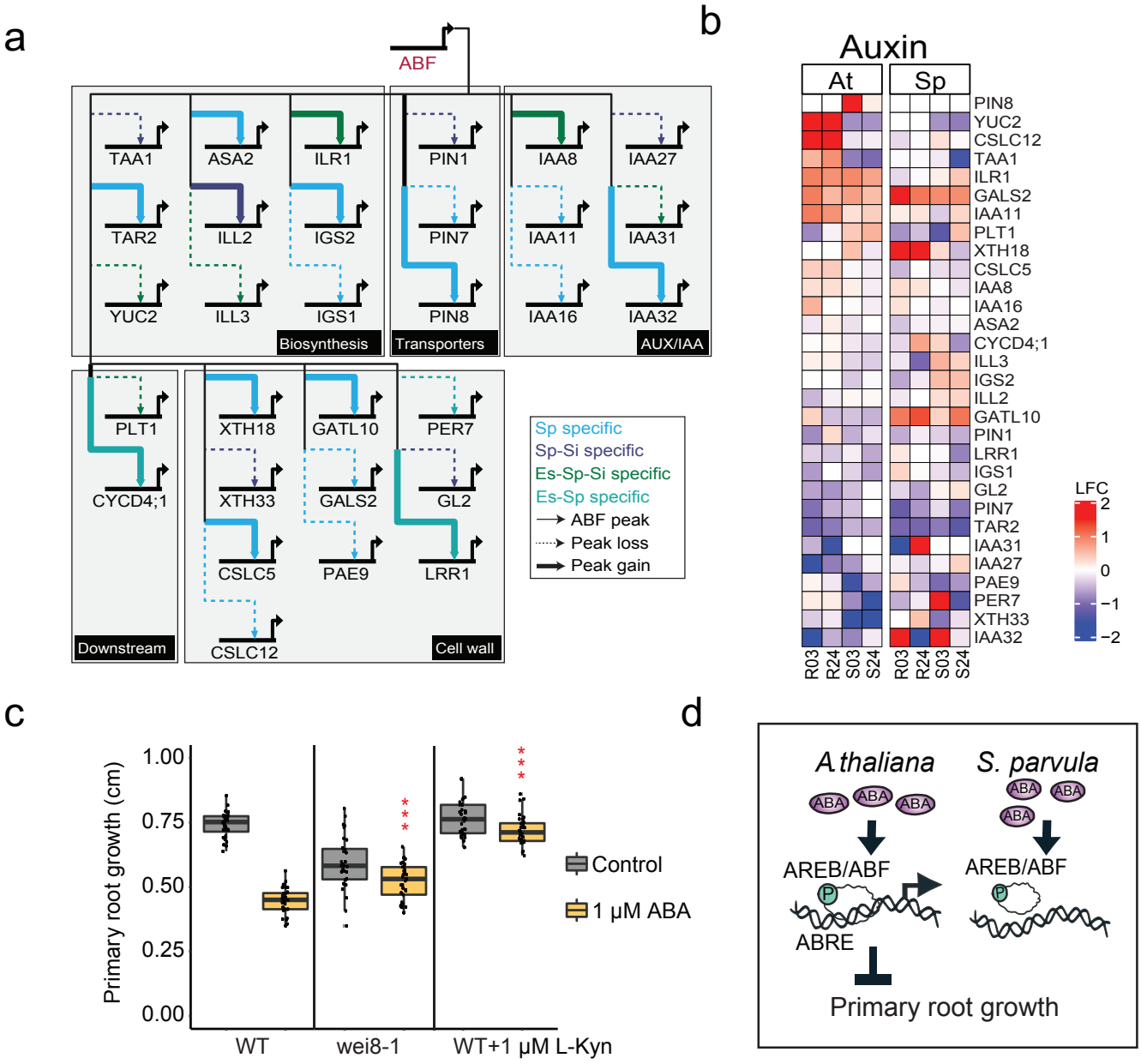
Figure 4: Rewiring of ABF-Auxin biosynthesis regulatory network is responsible for altered growth response in *S. parvula.*